International Journal of Pressure Vessels and Piping 86 (2009) 211–220

Contents lists available at ScienceDirect

International Journal of Pressure Vessels and Piping

journal homepage: www.elsevier.com/locate/ijpvp

Intergranular susceptibility in failures of high pressure tubes

Jose Luis Otegui [a], Pablo G. Fazzini [b,*], Juan Massone [c], Hugo Ortiz [c], Pablo Barcia [d], Guillermo Guidi [d]

[a] Welding and Fracture Division, INTEMA, CONICET, Juan B. Justo 4302, 7600 Mar del Plata, Buenos Aires, Argentina
[b] Gie S.A., Argentina
[c] Metallurgy Division, INTEMA, CONICET, Juan B. Justo 4302, 7600 Mar del Plata, Buenos Aires, Argentina
[d] Dow, Argentina

ARTICLE INFO

Article history:
Received 4 December 2007
Received in revised form
26 June 2008
Accepted 18 September 2008

Keywords:
High pressure
Thick steel tubes
Autofrettage
Intergranular cracking
Temper embrittlement

ABSTRACT

This work addresses the influence of metallurgical susceptibility to intergranular cracking on the repeated cracking and failure of thick wall curved steel tubes from a petrochemical reactor. These tubes are made of HP-4 steel, bent and heat treated, and then subjected to autofrettage. Internal pressure is around 250 MPa. All failures are characterized by strongly branched, mostly circumferential multiple intergranular cracks. Most cracks initiated in the outer surface, in contact with steam; these were related to stress corrosion cracking (SCC). Some cracks initiated in pre defects in the inner surface, in contact with a polymer, and in the mid thickness of the tube wall. This study includes the assessment of deformation and temperature induced embrittlement mechanisms, measurement of longitudinal residual stresses, and mechanical testing included tensile, Charpy and SCC tests. Susceptibility to intergranular cracking was experimentally assessed by recreating conditions of embrittlement by thermal treatments and tensile testing. Samples with 0, 3 and 5% plastic deformations were subjected to 24 h thermal treatments between 300 and 400 °C. Under the conditions of previous plastic deformation due to bending and autofrettage it was possible to recreate intergranular embrittlement at service temperatures, a phenomenon similar to temper embrittlement. The process of forming the bent created localized yielding and large longitudinal residual stresses. Recovery measures, mostly relying on thermal treatments, were defined.

1. Introduction

This study was carried out after repeated failures of thick wall curved steel tubes, used in a jacket type high pressure polymerization reactor, occurred between 2002 and 2005. The reactor is composed of individual tubes, bent to a J-shape, and joined together by bolted joints, see Fig. 1. The reactor has about 130 curved steel tubes, of diameters 113 mm OD and 51 mm ID. Along the whole length of the reactor, this inner tube transporting polymer is surrounded by an outer tube, between these, refrigerating treated water circulates. The diameter of each curve is around 2400 mm; the length of the tract up to the thread is 4200 mm. Within the tubes ethylene circulates in a polymerization stage (approximately ethylene 75%, polyethylene 25%); process water circulates outside the tubes.

The consequences of these failures involve unexpected plant stops, with concurrent production losses and maintenance costs. For about 20 years the reactor worked to a pressure of around 250 MPa, with approximately 45 stop and run cycles per year that is to say about 900 pressure cycles. Process valves produce low frequency fluid pulsations (1/25 Hz) of large amplitude (approximately 50 MPa); this is done to accelerate the process and to clean the inner walls of the tubes. The reactor also suffers from high frequency (20 Hz) and low amplitude pulsations due to the operation of a six cylinder compressor that rotates at 200 RPM. Nominal temperature of the tube is approximately 300 °C.

The chemical, mechanical and dimensional specifications correspond to Timken 4333M4 tubes (1970, 1976, revised 1979), see Tables 1, 2 [1]. This steel has high strength, due to high contents of C, Mn, Cr and Mo, and good ductility, due to 2% Ni. These tubes are manufactured by an electric arc, with degassing and deoxidation processes; then they are bent and subjected to quench and tempering heat treatments. Manufacturer data indicate that after the curving process the tubes are heat treated at 490 °C. The curved tubes are afterwards internally pressurized in order to assure plastic deformation of the material near the ID. This creates a circumferential residual stress field that is compressive near the ID and tensile near the OD. This is called autofrettage. The pressure is fine tuned according to the actual yield strength of each batch of tubes to increase the resistance to internal pressure; for these tubes, the autofrettage pressure is around 73.5 MPa.

* Corresponding author.
E-mail addresses: fazzini@giemdp.com.ar (J.L. Otegui), venturino@giemdp.com.ar (P.G. Fazzini).

0308-0161/$ – see front matter © 2008 Elsevier Ltd. All rights reserved.
doi:10.1016/j.ijpvp.2008.09.008

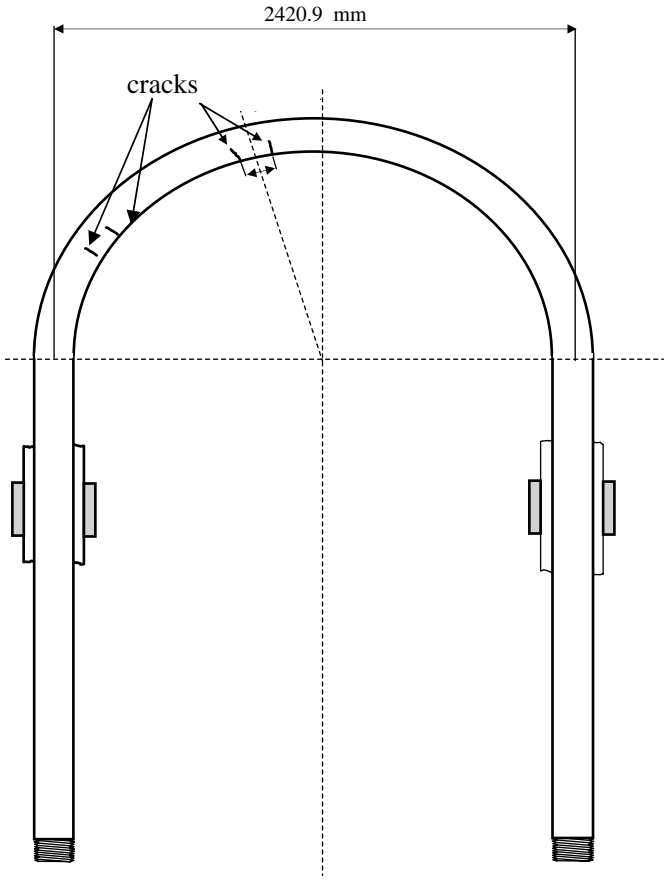

Fig. 1. Typical location of cracks in a curved tract of a reactor.

All failures are characterized by intergranular and branched cracks propagation, initiated in the curved sections (Fig. 1); no crack was detected on the straight parts [2]. Before 2004, cracks initiated at the outer surface (water side). Fig. 2a shows the results of black on white magnetic particles testing of the outer surface of the thick walled tube. Typical H-shaped branched crack can be seen. Subsequent ultrasonic mapping allowed recognizing typical crack branching and propagation in the pipe wall, see for example Fig. 2b. Smaller secondary cracks are not displayed in this sketch.

Initial failure analyses related these failures to a process of stress corrosion cracking, SCC. Acoustic emission tests carried out on back up tubes dismiss the possibility of cracks being initiated during storage. Crack propagation was considered a consequence of the combined action of poor water chemistry and high operating stresses. Stresses due to internal pressure, pipe support conditions and in-service expansions were modeled, and found to be high enough to justify the required crack driving forces. Alkaline agent Nalco 4025, forming Na(OH), was eventually replaced by morpholine.

Two of the last failures showed similar growth characteristics, but apparently initiated in the inner surface and in the mid thickness of the tube. These proved that previous assumptions did not fully explain the failure mechanism. Examples of Fig. 3a, b, c correspond to these three different failure types: (a) a typical failure before 2004, initiated at the outer surface; (b) curve 57 old (2004), initiated at the inner surface; and (c) curve 57 new (2004), initiated at mid thickness and failed after less than a month in a replacement tube. These last failures prompted a study to determine the weaknesses of the material that eventually favored the occurrence of failures, in order to define and implement effective mitigation measures.

Table 2
Mechanical properties of Timken tubes in a polymer reactor.

Tube	Yield strength (MPa)	UTS (MPa)	Elongation %	Area red. %
114 (2002)	1095	1188	10.5	57
Specification	980 min	1120 min	14 min	45 min

2. Dimensional, fractographic and metallographic analyses

A possible cause of the observed failures is the effect of the lateral impacts during the bending procedure of the curves, which could produce ovalizations in the tube and manufacturing residual stresses. Outer diameter measurements show a maximum difference of 1.7 mm, this is 1.5%. Inner diameter shows a maximum difference of 6.2 mm, this is 12%. Thickness shows a maximum difference of 2.5 mm, this is 7.5%. Specification establishes maximum tolerances in the thickness of ±5%. The thickness and outer diameter are within tolerance. It is observed that due to the rolling process from the outside, thickness variations are translated into variations of the inner diameter, the outer diameter being within very good dimensional tolerances. The manufacturing process did not produce dimensional variations above the specified tolerances.

As already mentioned (Fig. 2), all tubes failed due to the propagation of branched cracks in the curved section of the tubes. Many secondary cracks were detected in almost all the failed tubes, most of them initiated at the outer surface, which did not break the other surface of the pipe.

No matter what the initiation site was, subsequent propagation of the cracks was in all cases intergranular. Fig. 4 (×25) shows a scanning electron microscope (SEM) fractography of a typical intergranular crack propagation from a transgranular initiation site, shown vertical, to the left (curve 57, 2004). A black magnetite film is covering most of the crack surface. The optical metallography of Fig. 5 (×200) shows as an example a polished and 2% Nital etched cross section of curve 57, with a typical intergranular crack propagation in the martensitic material of the tube. Its initiation site had a typical fatigue aspect, although its surface was also covered by a black magnetite film. The micrograph also shows the acicular characteristic of a tempered martensitic microstructure. Two step colour etching for multiphase steels was used; first etching with 4% picral, and then etched using a 10% aqueous solution of sodium metabisulfite.

3. Chemical and mechanical tests

3.1. Compliance with specifications and assessment of material toughness

Tests were carried out to verify compliance with chemical and mechanical specifications, see Tables 1, 2. Elongation is in one case

Table 1
Chemical composition of Timken tubes in a polymer reactor.

Material	C	Mn	P	Si	Cr	Ni	Mo
Old curve #57	0.31	0.87	0.012	0.34	065	1.82	0.43
New tube #57	0.34	0.86	0.012	0.25	0.69	1.85	0.49
Curve 114	0.35	1.00			0.70	2.0	0.50
Specification	0.30–0.38	0.7–1.0	0.015 max	0.20–0.35	0.7–0.9	1.65–2.0	0.35–0.45

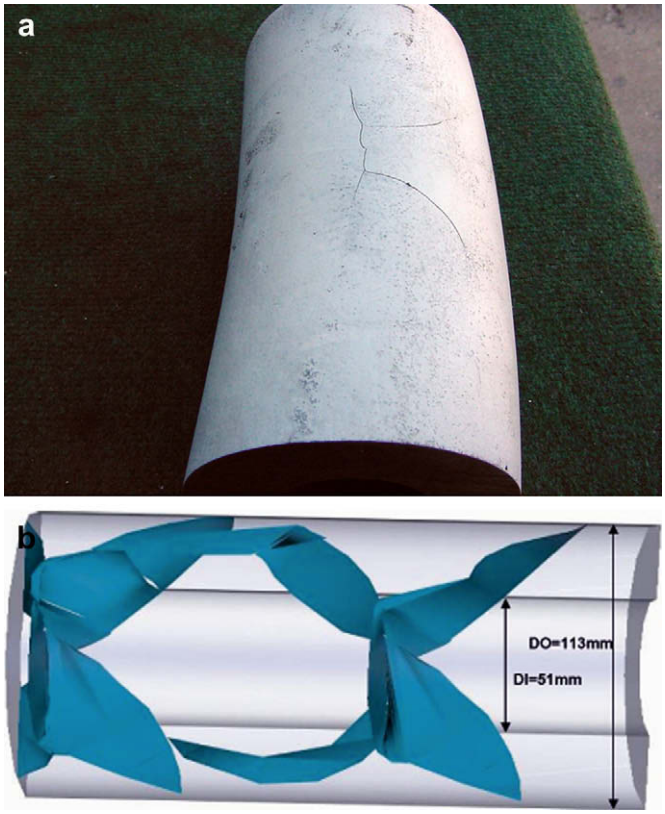

Fig. 2. (a) Typical H-shaped, branched crack, as seen in the outer surface of the thick walled tube. (b) Mapping of typical crack branching and propagation in the pipe wall.

below tolerance. Hardness values in all failed curves compared well with the specifications of AISI 4340 for fittings [3].

The possible incidence of embrittlement effects was investigated by means of Charpy impact tests at room temperature on ex-service samples. Specimens were taken from the straight tract of the tube and from the outer area of the curved sections. Table 3 summarizes the average values of several tests on uncracked specimens, and single results on specimens taken in the material close to the cracks. In one single case, a marked decrease in toughness was identified.

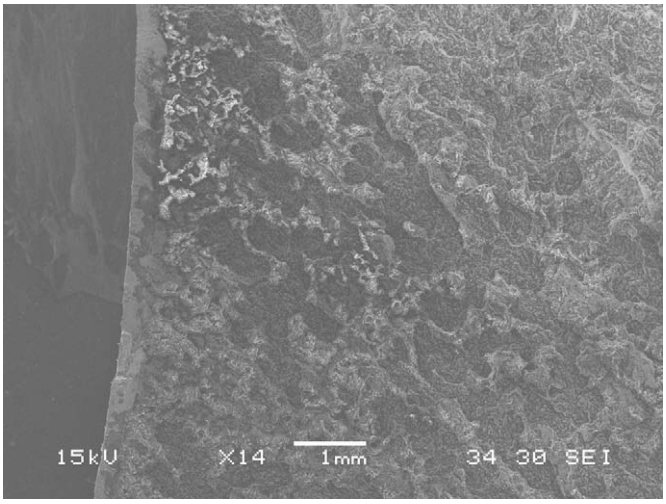

Fig. 4. SEM fractography of a typical intergranular crack propagation from a transgranular initiation site, shown vertical, to the left (curve 57, 2004) (×14).

These freshly broken fracture surfaces were then inspected in the SEM. Fig. 6 shows a typical fracture surface of a specimen from a cracked curve. All specimens show well developed shear lips close to three free surfaces, which justify the high values of impact energy, and which are apparently unaffected by any embrittlement. Even a small crack in a shear lip in one specimen did not result in a significant decrease of impact energy. In the 30% inner area, however, some differences were appreciated. Note in Fig. 8 how the fracture in this inner area propagated in a wavy pattern, that reveals a specific crack path related to the weakest microstructural features. As expected, the specimens with the smallest shear lips showed the lowest impact energies.

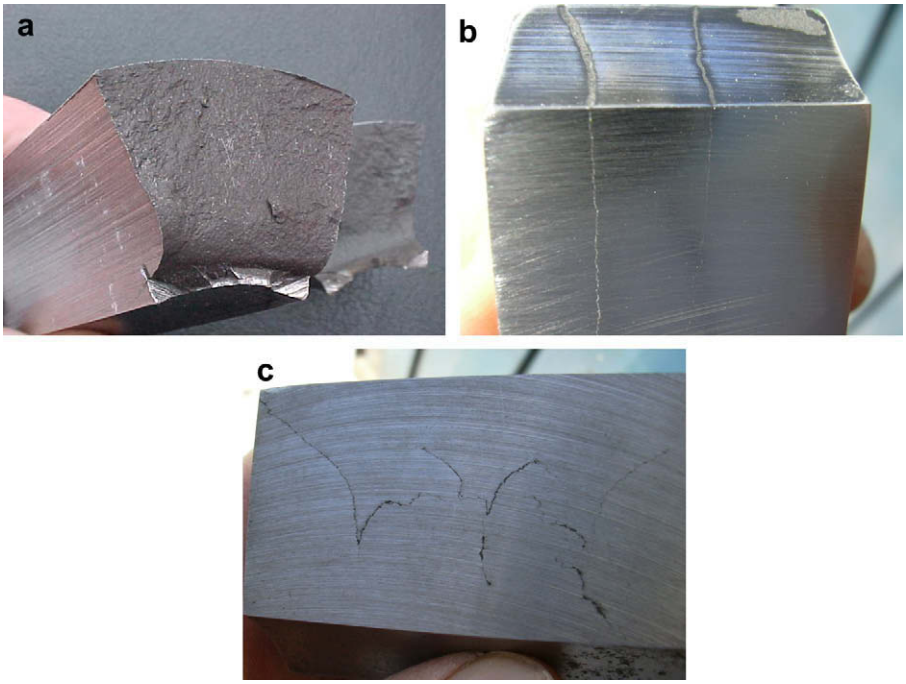

Fig. 3. Three cracks corresponding to different failures, initiated (a) at the outer surface, (b) at the inner surface, and (c) at mid thickness.

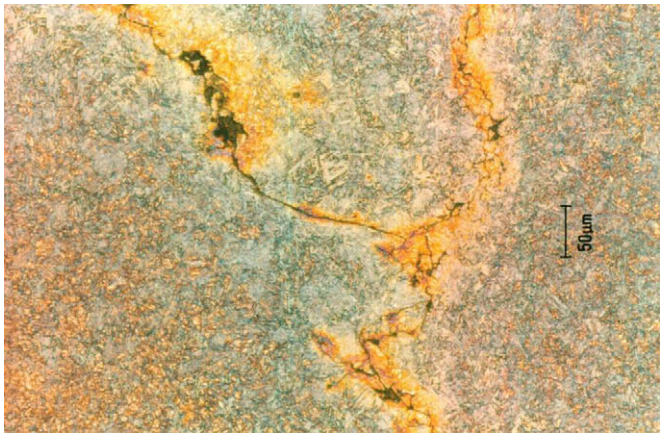

Fig. 5. Typical intergranular crack propagation in the martensitic material (curve 57, 2004) (×200).

Fig. 7 (×4000) shows the fracture surface in the inner area of the Charpy specimens from the straight tube. Note the micro void ductile fracture mechanism. Fig. 8 (a ×500, b ×4000) shows the fracture surface in the inner area of a specimen from a cracked curve (Fig. 6). Note that now the fracture surface is not flat. Although a micro void ductile fracture is also seen, secondary cracks are quite numerous. These secondary cracks were produced by the impact itself; no black films are seen in their surfaces.

3.2. Determination of residual stresses

Another possible cause for the observed failures is the effect of manufacturing (both circumferential and longitudinal) residual stresses. Residual stress analyses were carried out placing strain gauges in sections of two curves where cracks were observed, see Fig. 9. Strain gauges were placed in the inner diameter, in the mid thickness and in the outer diameter. A 5 m long tube with a 3 m straight tract and a curved end was cut at the beginning of the curve for measuring residual stresses. This way, the obtained results correspond to the stresses originated by the manufacturing process (included autofrettage) and installation (curve of the original pipe). Strain gauges (1)–(5) were placed in the outer wall, to measure longitudinal residual stresses. Once these stresses were measured, strain gauges (6)–(8) were placed, in the neutral axis and at 90°, in a radius that contains the internal point (1). Radial stresses were detected in two positions with strain gauges (22) and (23), in the radius that contains the neutral axis (point (3)). Having fixed the longitudinal strain gauges, the section was transversely cut.

Fig. 10a, b shows the measured (a) longitudinal and (b) circumferential residual stresses, respectively. The measured radial residual stresses are compressive, with a relative maximum value of around 80 MPa, near the mid thickness. Maximum circumferential residual stresses are 400 MPa, in compression; tensile maximum is only 70 MPa. The observed distributions according to the two radii show appreciable differences that can be associated to the overlapping of the processes of previous bending of the pipe and later autofrettage. These values of circumferential residual stresses relate well with those measured before in a slice of a curve: outer radius 64 MPa, mid thickness 68 MPa, inner radius 11 MPa.

The most relevant result is that relatively large longitudinal stresses were measured; the maximum tensile longitudinal stress is 340 MPa. The stress distribution obtained along half the perimeter can be directly associated with the plastic deformations generated during bending of the pipe to manufacture the curve. These stresses are comparable with the expected service stresses, so they could have contributed to the occurrence of the observed failures.

Table 3
Room temperature Charpy impact test results.

Specimen	Position	Room temp.	
		Impact energy (J)	
		Subsize 7 × 10	Std 10 × 10
Uncracked tube	Straight	55	78
	Curve	57	81
Curve 114	Near crack	30	42
New 57	Near crack	52	74

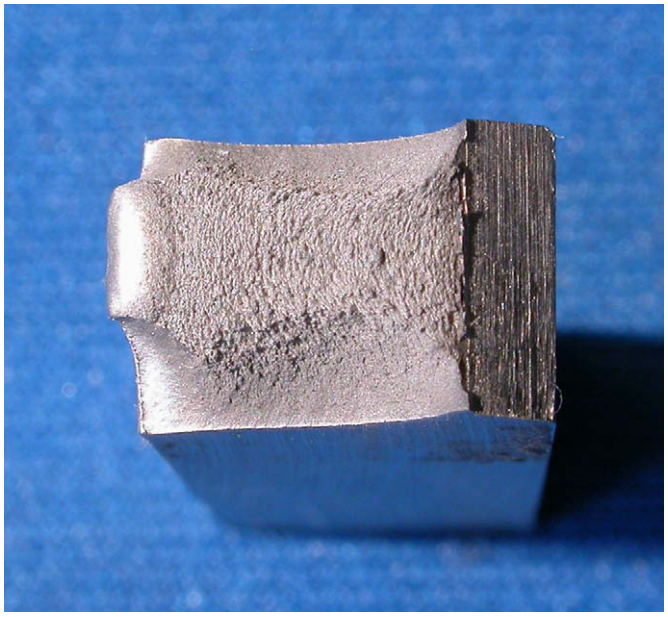

Fig. 6. Fracture surface of a specimen from a cracked curve.

4. Assessment of susceptibility to SCC

Stress corrosion cracking (SCC) is a phenomenon of time-dependent cracking that happens when three conditions are

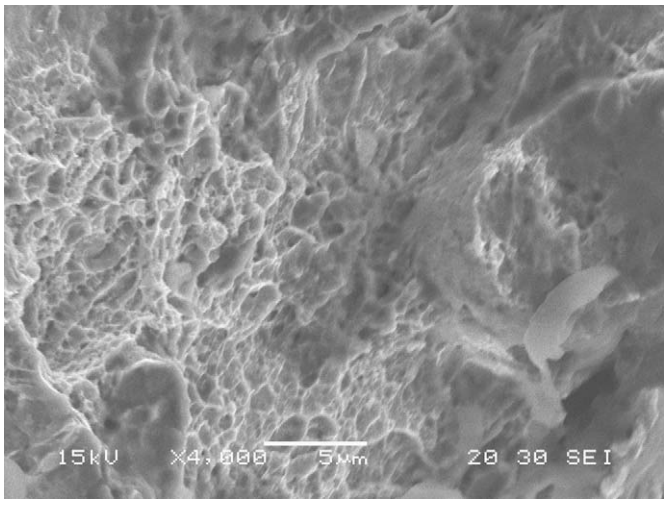

Fig. 7. Fracture surface in the inner area of the Charpy specimens from the straight tube (×4000).

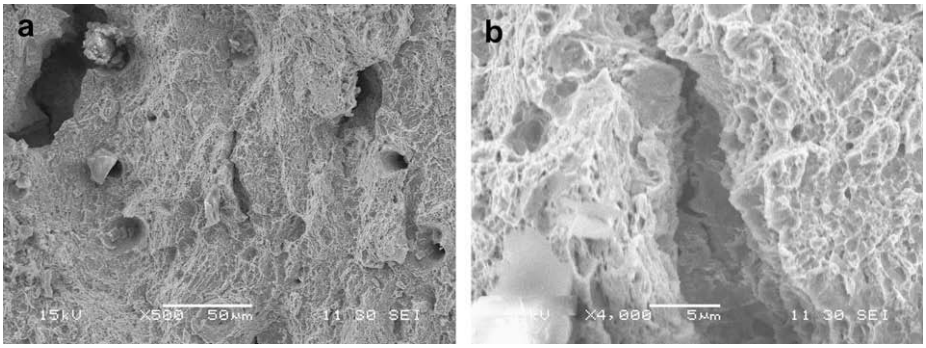

Fig. 8. Fracture surface in the inner area of a specimen from a cracked curve (a ×500, b ×4000).

met: the alloy is susceptible, its surface is exposed to a specific aggressive atmosphere, and the traction stresses are above a threshold level. The alkaline agent in the refrigerating water was suspected as a possible cause of cracking from the OD, a mechanism also called caustic attack or caustic embrittlement. The pH of the cooling water stayed around 10 during long periods of operation.

A series of tests were carried out in order to identify any possible particular susceptibility of the material to this in-service degradation process. The SCC test method involves tapered tensile test specimens that are subjected to tensile stresses immersed in the appropriate electrochemical conditions. It is based on the method developed by the American Gas Association [4]. These tests allow obtaining the following data for each material:

- threshold stress σ_{TH}: stress below which no cracks initiate;
- crack propagation rate.

Tapered specimens were cut from an uncracked material sample. The applied load was defined in order to apply a stress around 80% of yielding in the smallest section (neck). This allows embracing a wide stress spectrum, including all operating conditions. The specimens were subjected to 1-h-cycle tensile stresses in a "walking beam" test machine. It is generally acknowledged that higher temperatures bring higher SCC susceptibility. Temperature was set at 74 °C, to accelerate the test while preventing evaporation and decomposition of the solution.

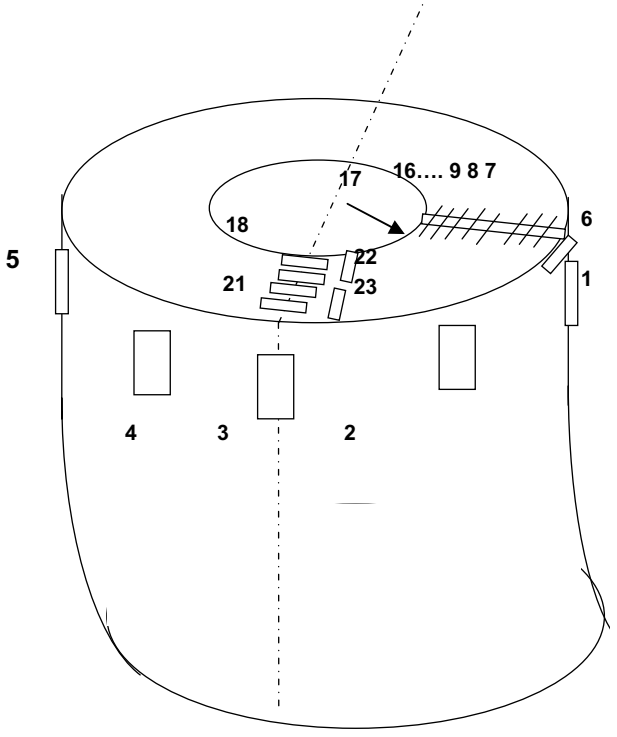

Fig. 9. Residual stress analyses were carried out placing strain gauges in sections of two curves where cracks were observed.

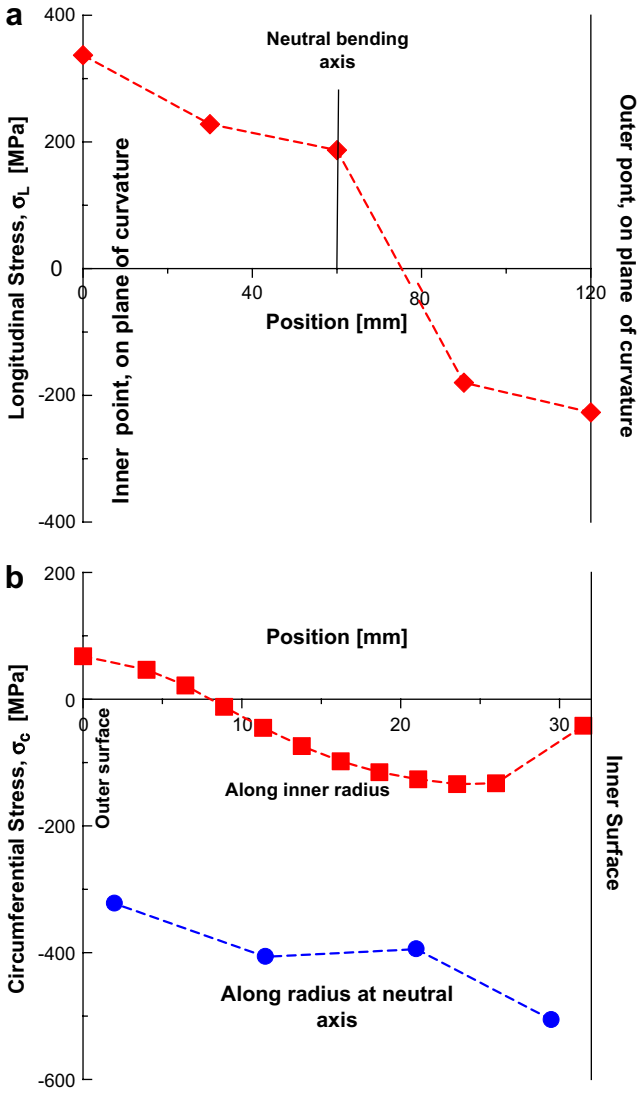

Fig. 10. (a) Longitudinal residual stresses. (b) Circumferential residual stresses.

The chemical composition of the solution in the electrochemical cell surrounding the specimen was NaOH 4.65 M. The pH measured at room temperature was far from 14. The potential was maintained constant at −850 mV with respect to saturated calomel (SCE), range reported as giving the highest susceptibility to caustic SCC. Stability of the reference electrode was checked before and after each test. The saturated calomel reference electrode was maintained below 60 °C, communicated to the cell by a Luggin capillary. The experimental set up was completed with an electrochemical cell made of carbon steel that acted as a counter electrode.

No cracks were detected during ultrasonic NDT and optical microscopy inspections (100×), although fluorescent magnetic particles had revealed potential defects in the neck. Although the pH of the cooling water stayed around 10 during long periods of operation, the material was not particularly susceptible to SCC that originated in the chemistry of the cooling water.

5. Assessment of the thermal mechanical embrittlement mechanism

Tempered martensite embrittlement (TME) can be classified into two types depending on the fracture mode: intergranular and transgranular TME. Transgranular TME was detected at test temperatures close to the ductile–brittle transition temperature. The phenomenon was related to the formation of coarse carbides at the martensite lath boundaries [5,6]; nevertheless some authors do not agree with this theory and attribute transgranular TME to the decomposition of retained austenite instead of the carbide coarsening [7]. The intergranular type of TME has been observed generally at test temperatures below the transition temperature and was associated with the combined action of coarse carbides and impurities at the prior austenite grain boundaries. If the grain boundaries act as slip barriers, the blocked slip bands can induce the crack nucleation at the grain boundaries [8,9].

The influence that previous plastic deformation exercises upon the toughness of the tempered martensite was evaluated being subjected to thermal cycles in the range of service temperatures of the reactor. This included to subject the characteristic martensitic structure of the tubes to plastic deformation and temperatures similar to those of service and to evaluate their influence on mechanical properties. Tensile tests were carried out in specimens taken from the straight tract of the tube, in specimens with the original (not deformed) material properties and in plastically deformed specimens, previously maintained at the test temperature.

Tensile specimens satisfy the standard ASTM E8-57T. It was made sure that the only plastic deformation in the specimens would be the one introduced in the laboratory in each sample. Plastic deformations were 3% and 5%. Later on, the specimens were subjected to temperatures of 300, 325, 350 and 375 °C during 24 h, and finally tensile tested to break. Fracture surfaces of the tested specimens were observed by SEM and optical microscopy. Tensile tests were also carried out on a specimen maintained for 24 h at 325 °C without previous plastic deformation, and on a specimen 5% plastically deformed and maintained at 520 °C for 24 h. Finally, two tensile tests with notched specimens were carried out, one of the original material and the other one with a plastic deformation of 5% and a maintenance at 325 °C during 24 h before the test. Specimens are listed in Table 4, with their corresponding number, the applied percentage of plastic deformation and the temperature to which each one was subjected.

Fig. 11a shows the load–deformation curve of the material in its original state (specimen #1). The material shows low strain hardening which results in an ultimate tensile stress (UTS) very close to the yielding. The specimens subjected to plastic deformation and temperature show a tensile behaviour very different to that of the original material. The specimens deformed 5% present a larger yield stress, as expected, but also showed some unexpected behaviour. For all maintenance temperatures, when reaching the yielding load the specimens destabilized, that is to say, yielding coincides with the peak load and in that point necking takes place. By way of example, Fig. 11b shows the load–elongation curve of specimen #4. Ductility is reduced in all cases down to 8%, from the original material ductility of almost 16%.

Table 4
Tensile tests on artificially embrittled specimens.

Specimen %	Deformat %	Temperature °C, 24 h			
		300	325	350	375
1	Material in original condition				
2	5	X			
3	5		X		
4	5			X	
5	5				X
6	3	X			
7	3		X		
8	3			X	
9 Notched	5		X		
10			X		
14 Notched	Material in original condition				
15	5	Maintained 24 h at 520 °C			
16	5	Maintained 24 h at 490 °C, air cooled, then at 325 °C for 24 h			

The same behaviour was obtained with specimens with 3% deformation. The decrease of load was always almost coincident with the elastic straight line, evidencing that the plastic deformation of the specimens is minimum, and all the deformation is due to necking. This behaviour would be critical if for some reason the material is imposed to a restriction of plastic flow, as happens in the middle area of the cross section. To evaluate this phenomenon, a test on a specimen deformed 5% and maintained for 24 h at 325 °C was carried out, in which a slot or circumferential notch was practiced (specimen #9).

Fig. 12a shows the tensile curve. As in the previous cases, yielding coincides with the peak load and immediately later an abrupt fall of the load takes place. When imposing a restriction to necking the specimen breaks practically without plastic deformation (0.8%). In the same test in the original material (specimen #14, Fig. 12b), embrittlement is not evidenced; the reduction in elongation is due to the stress raising and triaxiality effect of the slot.

To verify whether the phenomenon of embrittlement is produced by a combination of plastic deformation and temperature or only by one of these factors, a test on a specimen without previous plastic deformation and subjected for 24 h to 325 °C was carried out (specimen #10). The resulting curve is entirely comparable to that of the original material, with a deformation to break of 15.3% and an UTS of 1210 MPa. It is possible to conclude that the evidenced phenomenon of embrittlement is due to a combination of both parameters: plastic deformation and maintenance to temperature.

To verify if the embrittlement phenomenon is only manifested in the range of 300–400 °C, a 5% deformed specimen was tested after maintenance to 520 °C (specimen #15). Embrittlement does not take place for this maintenance temperature; deformation and UTS are identical to the material in its original state. Lastly, it was verified if the embrittlement phenomenon is destroyed by the thermal treatment after bending of the curves at 490 °C. Test 16 (Table 4) was carried out on a specimen 5% deformed, then maintained at 490 °C during 24 h, air cooled, and then taken to the embrittlement temperature (325 °C) during 24 h. The specimen was tested similarly to the others, at room temperature after air cooling. Embrittlement does not take place in this condition.

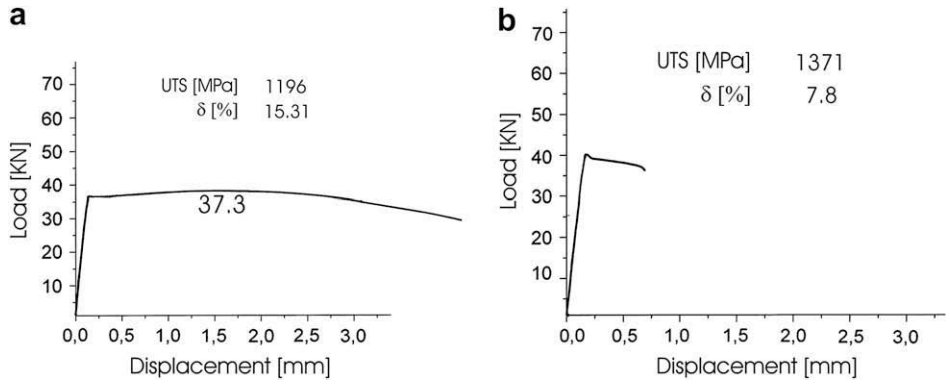

Fig. 11. (a) Deformation curve of the material in its original state, specimen # 1. (b) Load–elongation curve of specimen #4.

A microstructural characterization was carried out after testing, in samples from original and embrittled materials. An important content of globular inclusions was seen, which is representative of the analyzed material. No lengthened inclusions in the lamination direction were observed. Careful observations, carried out to larger magnifications, did not reveal the presence of precipitates, which would in principle be responsible for the embrittlement phenomena evidenced in this sample.

Fig. 13 (×1000) shows the microstructure of the original material, characteristic of the quenched and tempered steels with this chemical composition. This microstructure was not modified when subjecting the specimen to plastic deformation and temperature. The microstructure continues being typical of tempered martensite; consequently, the changes taking place in the material should be at a sub-microscopic level, not being possible to identify them under the available laboratory conditions.

Fracture surfaces in the original material show a rosette fracture type, typical in steels subjected to tension (Fig. 14). It exhibits three areas clearly distinguishable: a planar and fibrous inner area (A), a radial buffer area (B) and an outer ring (C).

The fibrous central area is where the fracture originates; it is the region of slow and stable (sub-critical) growth of the crack, which requires high energy. It has an appearance of fibres at random with micro voids in the whole surface. This area is seen at larger magnifications in Fig. 14a; longitudinal cracks are revealed. This is a characteristic peculiar of this material and it does not fit bibliographical descriptions. The radial area (B) is where the crack growth rate becomes fast or unstable. These marks trace the crack growth direction, both from the borders of the fibrous area or from their own origin, see details in Fig. 14b.

The outer area (shear lip) is an annular flat area adjacent to the free surface of the specimen, clearly distinguishable in this sample. The micro voids (dimples) in this area are smaller than those in the two previous areas. This is directly related with the variation in the distribution of inclusions. A detailed explanation of this characteristic of the material is given in Section 6.

The fracture surfaces of the embrittled samples do not present marked differences related with the amount of deformation or the maintenance temperature. In all cases the fracture continues being of the rosette type, with the three areas previously described clearly visible. These deformed samples have a radial area with a great quantity of longitudinal cracks that define a more irregular fracture path, with more crests and valleys. Differences were also observed in the size of the fibrous central area; a clear tendency of the size of the central area with the percentage of deformation or maintenance temperature could not be determined.

Fracture surfaces change in the case of notched tensile specimens. Fig. 15 corresponds to the original material, tested with a 0.65 mm deep, 55° Charpy-like notch. The fibrous central area remains, but the radial area and the outer ring disappear. These are replaced by an area with circumferential crests (ridges), concentric with the central and fibrous area normal to the propagation of the crack from mid thickness until the surface of the sample. As in the previous observations, the central area presents a great quantity of small cracks. Fig. 16 shows the fracture surface of specimen #9, tested with the same slot, but with a previous 5% plastic deformation and a temperature of 325 °C during 24 h. The central fibrous area disappears almost totally; only circumferential waves are observed in the propagation direction.

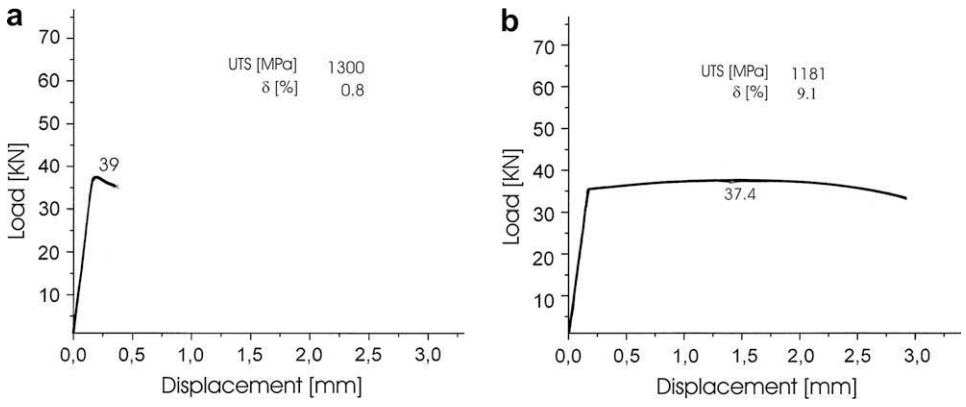

Fig. 12. Tensile curve.

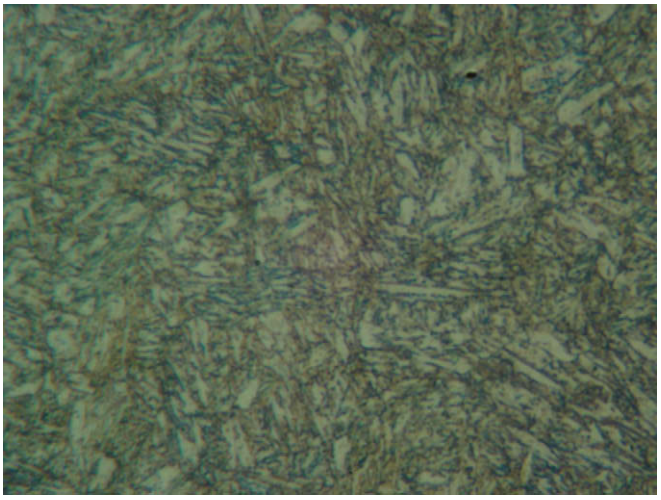

Fig. 13. Microstructure of the original material (×1000).

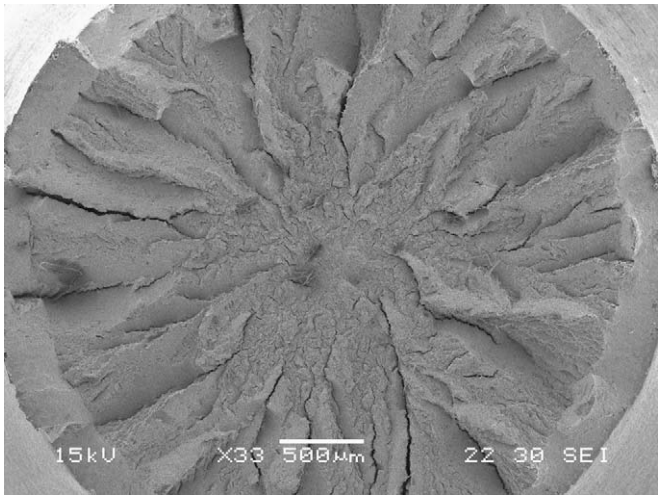

Fig. 15. Fracture surfaces in the case of notched tensile specimens.

6. Discussion of results

All failures are characterized by intergranular, strongly branched multiple cracks that are mostly circumferential. No particular susceptibility of this material to SCC was found. From the operational point of view, it is believed that this "racetrack configuration vessel" was at some time running either not full of water or boiling it away at the water high-line points. This justifies cracking from the OD on the upper side of the bends, because they are field-mounted in a dual-tilted angle position. This type of OD damage could have taken place initially years ago under different operating conditions, such as those following the reduction of water flow in the after cooler.

Similar attack had been reported on other reactors and high temperature HP coolers, where there was OD tube metal exposure above the water line [10]. It is one of the most vulnerable locations in the boiling water (BWS) system since the tube OD is under operating stress, and simultaneously exposed to the volatile environment of the BWS. Reportedly this type of damage is not common in other configurations of the reactor, such as those of the hanging loop design. Avoiding this type of SCC attack from the OD requires significant precautions to be certain that the tubes always operate with the jackets water full, i.e. monitoring balances, flows and pressures.

The last two failed tubes changed this pattern. After many years of service, cracks in curve 57 initiated in pre existing cracks in the inner (polymer) surface of the tube (ID). Oddly enough, the replacing tube failed only after one month in service. Cracks in this new curved tube began in the middle of the thickness of the tube wall.

In all cases the cracks propagated under the action of service loads, which provoked tensile and bending stresses due to the

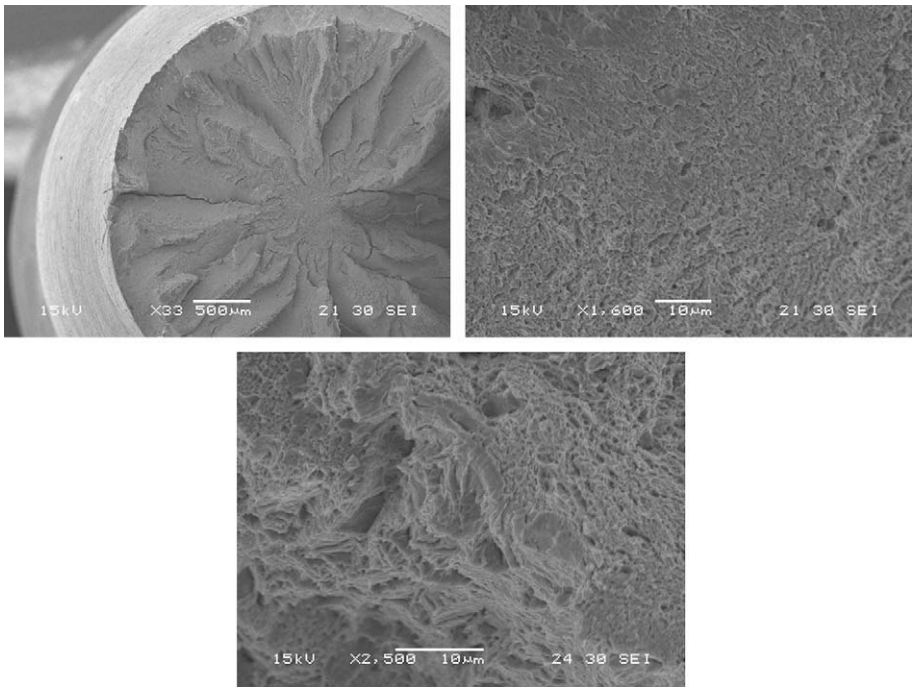

Fig. 14. Rosette fracture type.

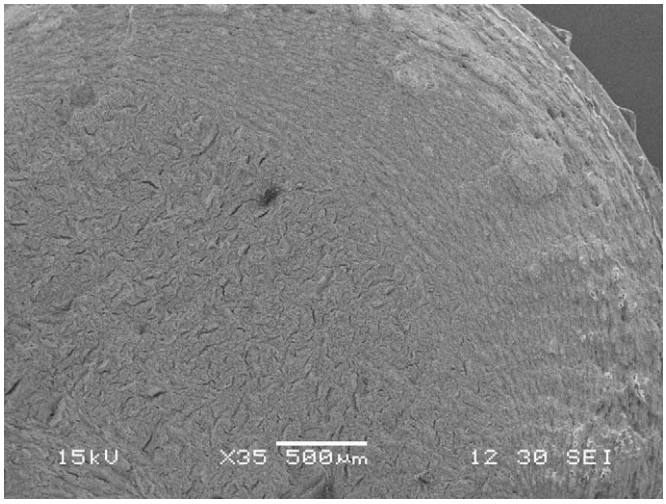

Fig. 16. Fracture surface of specimen #9.

combination of thermal and mechanical expansion and internal pressure, as well as torsion moments originated by support conditions of the pipe and in-service expansions. The fabrication process added large residual stresses in localized regions of the curved tracts (Section 3). These high residual stresses are not the only fabrication-related influence on the repeated failures. It is apparent that the material of the reactor tubes suffered embrittlement mechanisms in the grain boundary that made them susceptible to intergranular cracking, in some cases with very high propagation rates.

This material presents a totally martensitic matrix, tempered at low temperature. There is evidence in technical bibliography that tempered martensitic steels are susceptible to suffer intergranular embrittlement [11]. This susceptibility has been experimentally verified in this study (Section 6), in specimens under thermal and mechanical conditions similar to those prior to placement in the reactor. The material embrittled by the combined effect of plastic deformation and temperature. The phenomenon was seen with deformations of 3% and 5%, and temperatures between 300 and 375 °C. The maintenance to temperature per se (without plastic deformation), does not produce embrittlement. Larger temperatures (520 °C) did not embrittle the deformed structure. This embrittlement is very localized to the cracked areas; note that Charpy results in specimens from curved regions did not show large differences from those corresponding to the straight regions.

The extremely low capacity for strain hardening of the tube material provokes plastic collapse immediately after reaching the material's elastic limit. In other words, the material collapses plastically whenever plastic deformations are required. That is why all cracks grow by micro void coalesce, a mechanism that is typical of ductile fractures, but with very little overall deformation. This lack of strain hardening is especially important in conditions of plane strain, when the material is forced to yield in a triaxial state of tensile stresses. Restriction to plastic flow, as induced in the laboratory using notched specimens, makes the phenomenon critical. This restriction occurs in service at the mid thickness of the tubes, which is why cracks initiated in the middle of replacement tube #57, without any apparent initiation defect.

Intergranular embrittlement is associated with a relatively short (at least an hour) exposition to temperatures between 200 and 350 °C. Because it is mostly found in temper treatments, it is usually called tempered martensite embrittlement. In the case under study, embrittlement was most probably not produced in any measurable amount during actual tempering, but at the operating temperatures. In this case, a considerably longer time was available for intergranular embrittlement and ongoing cracking.

Inspection did not detect any manufacturing deficiencies. The industry's experience is that operating with 4333M6 tubes instead of 4333M4 tubes did not reduce failure rates. The higher alloy 4333M6 HP tubes are significantly stronger but also are more prone to cracking in reactor applications. Other manufacturers experienced cracking failure problems with M6 tubing since its introduction; the manufacturer of curved tubes does not recommend using 4333M6 for reactor tubing.

Why a grain boundary embrittlement mechanism took place in these tubes and not in others of similar reactors is clearly related to the fabrication sequence. The straight tubes are first bent, by means of hydraulic jacks that load the tubes in specific, localized sections. Then the tubes are subjected to a stress relief heat treatment at 490 °C. Test 16 (Section 6) shows that this treatment, if carried out for a sufficiently long time, eliminates the effect of plastic deformations during bending on intergranular embrittlement. The curved tubes are afterwards pressurized to an internal pressure that assures plastic deformation of the material near the ID.

The key is having the autofrettage after curving. Both processes involve localized plastic deformations. During autofrettage the curves tend to straighten, as in a barometer. In this process the material is again deformed plastically, and residual stresses are generated, which are tensile in the longitudinal direction, of up to 330 MPa (Section 3). The plastic deformations, although small, seem to have been enough to increase the susceptibility of the material, since martensite does not have a large ductility.

The compressive residual stresses arising from an autofrettage treatment have long been exploited to enhance the fatigue life of process piping. The elastic–plastic deformation during bending of a thick walled cylinder results in a residual, axial stress distribution. When the bent pipe receives an autofrettage treatment without an intermediate heat treatment, this produces a further residual, triaxial stress state. A recent study [12] shows that large plastic penetrations arising from bending and autofrettage can residually stress the section beyond its yield point. In each unloading the Bauschinger effect could reduce the yield point and lead to reversed plasticity. The work by D. Rees agrees with the findings of the present study, in that interacting residual stresses result in an axial stress as important as the hoop stress under service loadings.

In curves without cracks, this embrittlement mechanism is reversible with a new quench and temper thermal treatment. This could lead to a method of mitigation and recovery of degraded but not yet cracked tubes. Another important factor to reduce the risk of further failures in replacement tubes is to ensure that new tracts are placed free of large longitudinal stresses originated in the restraint and stiffness of the rest of the reactor. The tubes should not undergo plastic deformation if later in service they work at temperatures in the interval 300–400 °C; therefore it was not recommended to carry out the autofrettage process. It is impossible to avoid plastic deformation, during the forming of the curves then appropriate thermal treatments should be carried out to erase the effect of this plastic deformation.

It is concluded that cracking was promoted by an inherent weakness in the grain boundary of the tube material. Initiation of actual cracks depended on where specific geometric discontinuities were present (roughness in the outer surface, a small circumferential crack in the inner surface, an inclusion or void in the material, etc.). Autofrettage increased the material's susceptibility to intergranular cracking. This is not related to the circumferential stress field deliberately provoked by the process; these stresses are typically lost after 5 years of reactor operation, due to prolonged pressure at a relatively high temperature (a sort of in-service stress relief treatment). Therefore, the imposed stresses found in these

autofrettage tubes would be long gone for most of the reported failures.

The re-autofrettage pressure is not very controllable in these tubes, because the difference between the yielding and ultimate strengths is small. It is reasonable that the autofrettage stress falls with time. A better alternative is to replace tubes by new ones with no autofrettage. A stress analysis would be needed to verify the compliance of stresses derived from inner pressure in these new conditions. Changing the curving method to a more controlled, homogeneous one will probably be also useful, since plastic deformations and residual stresses are larger where there is a localized deformation.

7. Conclusions

Experimental evidence indicates that one common root cause for failures is a mechanism of degradation in the grain boundary, denominated temper embrittlement, which in this case has taken place during service, in the range of working temperatures. The embrittlement mechanism can be related to the fabrication sequence. The straight tubes are first bent, then stress relief heat treated. During autofrettage after curving the material is again deformed plastically, and large longitudinal residual stresses are generated.

Susceptibility to intergranular cracking was experimentally assessed by recreating conditions of embrittlement by thermal treatments and tensile testing. It was found that under the combination of plastic deformation during fabrication and later service temperatures the material loses strength just after yielding. In this condition the material is unable to sustain the stresses above yielding under conditions of restricted plastic deformation, as occurs in the plane deformation stress states. These occur in the presence of defects and in the mid thickness. This does not occur in a material without previous plastic deformation (not subjected to autofrettage).

Without cracks this embrittlement mechanism is reversible with a new quench and temper thermal treatment. It is recommended to carry out a specific study to define an appropriate thermal cycle to reverse the embrittlement phenomenon.

Re-autofrettage is not recommended, it is difficult to control and in any case it has been shown that autofrettage stresses fall with time in service. A stress analysis would be needed to verify the compliance of stresses derived from inner pressure in these new conditions. Changing to a more controlled, homogeneous curving method could reduce localized plastic deformations and residual stresses. It is also recommended to develop a procedure to ensure low constraint stresses when replacing tubes.

Autofrettage increased the susceptibility to cracking by causing plastic deformation. Although no general advice can be given, it is clear that for some materials and service conditions autofrettage may not be recommended. One reason is that the plastic strain induced can be damaging, as in this case, if the material is susceptible. There is also some evidence that after a certain service life at high temperatures and pressures the beneficial residual stress can become substantially relieved, reducing the enhanced fatigue life intended with the fabrication process.

References

[1] Practical data handbook for metallurgists. Timken steel online services, <www.timken.com>; 2007.
[2] Assessment of material embrittlement on repeated cracking in polymerization reactor. Technical report GIE 2803-02-05. Dow Chemical; 2006.
[3] Banerjee B. The mechanical threshold stress model for various tempers of AISI 4340 steel. University of Utah; Aug 2005.
[4] Test method for defining susceptibility of pipeline steels to stress-corrosion-cracking. NG-18 report 146. American Gas Association; 1985.
[5] Krauss G. Steels: heat treatment and processing principles. ASM International; 1990. p. 231.
[6] Kwon H, Kim CH. Variation of brittle fracture with test temperature in tempered martensitic structure in 2Si−0.4C steel. Metallurgical and Materials Transactions A 1983;14:1389.
[7] Peters JA, Beeb JV, Kolk B, Garrett G. Acta Metallurgica 1989;37:675.
[8] Lee KB, Yoon SH, Hong SI, Kwon H. On intergranular tempered martensite embrittlement. Scripta Metallurgica et Materialia 1995;32(8):1197.
[9] Briant CL, Banerji SK. The fracture behavior of quenched and tempered manganese steels. Metallurgical and Materials Transactions A 1982;13:827.
[10] L. Barcia, M.J. Schmidt. Product cooler tube failures in Bahía Blanca LDPE train. SPI technology transfer workshop V: process safety in the high pressure polyethylene industry. Houston; 2003.
[11] API RP 934 Materials and fabrication requirements for 2-1/4Cr-1Mo and 3Cr-1Mo steel heavy wall pressure vessels for high temperature, high pressure hydrogen service. American Petroleum Institute; 2000.
[12] Rees DWA. Autofrettage of thick-walled pipe bends. International Journal of Mechanical Sciences 2004;46:1675.